Published in final edited form as:

Nat Chem Biol. 2016 October ; 12(10): 787–794. doi:10.1038/nchembio.2147.

An histidine covalent receptor/butenolide complex mediates strigolactone perception

Alexandre de Saint Germain[#1,2,3], **Guillaume Clavé**[#4], **Marie-Ange Badet-Denisot**[4], **Jean-Paul Pillot**[1], **David Cornu**[5], **Jean-Pierre Le Caer**[4], **Marco Burger**[2,3], **Frank Pelissier**[4], **Pascal Retailleau**[4], **Colin Turnbull**[6], **Sandrine Bonhomme**[1], **Joanne Chory**[2,3,*], **Catherine Rameau**[1,*], and **François-Didier Boyer**[1,4,*]

[1]Institut Jean-Pierre Bourgin, INRA, AgroParisTech, CNRS, Université Paris-Saclay, RD10, 78026 Versailles Cedex, France

[2]Howard Hughes Medical Institute

[3]Plant Biology Laboratory, The Salk Institute for Biological Studies, La Jolla, CA 92037, USA

[4]Institut de Chimie des Substances Naturelles, CNRS UPR2301, Univ. Paris-Sud, Université Paris-Saclay, 1 av. de la Terrasse, F-91198 Gif-sur-Yvette, France

[5]Institut de Biologie Intégrative de la Cellule, CNRS, CEA, Univ. Paris-Sud, Université Paris-Saclay, 1 av. de la Terrasse, F-91190 Gif-sur-Yvette, France

[6]Division of Cell and Molecular Biology, Imperial College London, London SW7 2AZ, United Kingdom

[#] These authors contributed equally to this work.

Abstract

Strigolactone plant hormones control plant architecture and are key players in both symbiotic and parasitic interactions. They contain an ABC tricyclic lactone connected to a butenolide group, the D-ring. The DWARF14 (D14) strigolactone receptor belongs to the superfamily of α/β-hydrolases and is known to hydrolyze the bond between the ABC lactone and the D-ring. Here we characterize the binding and catalytic functions of RAMOSUS3 (RMS3), the *pea* (*Pisum sativum*)

[*]Corresponding authors: francois-didier.boyer@cnrs.fr, Catherine.Rameau@versailles.inra.fr, and chory@salk.edu.

Author contributions

A.dS.G., G.C., J.C., C.R., F.-D.B. designed research; G.C. designed and synthesized the probes; G.C., F-D.B. synthesized the other chemicals; A.dS.G., M.-A.B.-D. produced and purified the proteins; A.dS.G. characterized the proteins; A.dS.G., G.C. did the kinetic experiments; A.dS.G., J.-P.P., S.B., C.R., F.-D.B. performed the plant experiments; D.C., J.-P.L. performed the mass experiments; G.C., F.P., F.-D.B. performed the HPLC analyses and separations; P.R. did the x-ray analyses; M. B. did the protein modeling; C.T. performed strigolactone quantifications in pea; A.dS.G., G.C., M.-A.B.-D., J.-P.L., P.R., C.T., J.C., S.B., C.R., F.-D.B. analyzed data; A.dS.G., C.R., F.-D.B. wrote the paper.

Competing financial interests

The authors declare no competing financial interests.

Accession Numbers. Sequence data from this article can be found in the *Arabidopsis* Genome Initiative or GenBank/EMBL databases under the following accession numbers: RMS3_Terese (KT321518), RMS3_T2-30 (KT321519), RMS3_M2T-32 (KT321520), RMS3_Torsdag (KT321521), RMS3_K487 (KT321522), RMS3_K564 (KT321523), RMS3_Raman (KT321524), RMS3_WL6042 (KT321525), AtD14 (At3g03990), AtHTL (At4g37470), AtMES9 (At4g37150).

ortholog of rice (*Oryza sativa*) D14 strigolactone receptor. Using novel profluorescent probes with strigolactone-like bioactivity, we show that RMS3 acts as a single-turnover enzyme that explains its apparent low enzymatic rate. We further demonstrate the formation of a covalent RMS3/D-ring complex, essential for bioactivity, in which the D-ring is attached to Histidine 247 of the catalytic triad. These results reveal an undescribed mechanism of plant hormone reception where the receptor performs an irreversible enzymatic reaction to generate its own ligand.

Introduction

In the last ten years, there have been major advances in understanding plant hormone signaling, including for the last discovered class, the strigolactones (SLs). SLs were initially identified in the rhizosphere as key signals in both symbiotic and parasitic interactions[1]. SLs have since been shown to affect shoot branching and many other traits[2-4]. All natural SLs contain a tricyclic lactone (ABC rings) connected via an enol ether bridge to a butenolide group (the D-ring) with a 2*R'* configuration and a methyl group at 4' position (**Fig. 1a**). The conserved CD component is essential for hormonal bioactivity, whereas changes in the A and B rings are tolerated[5].

SL receptors (D14 in rice, AtD14 in *A. thaliana*, DAD2 in petunia (*Petunia hybrida*)) belong to the α/β-fold hydrolase superfamily and contain the Ser, His, Asp catalytic triad located in a hydrophobic active site[6]. Binding of the synthetic SL analog GR24 (**Fig. 1a**) to the SL receptor is thought to involve hydrogen bonds and hydrophobic interactions with pocket residues of D14. GR24 is then hydrolyzed, yielding inactive ABC and 5-hydroxy-3-methylbutenolide (D-OH) products[6]. However, the enzymatic activity of the SL receptor appears to be very slow[6,7] and its role in SL perception is unclear. It has been suggested that SL binding and hydrolysis in SL perception would destabilize the SL receptor[8], promoting recruitment of the MORE AXILLARY GROWTH2 (MAX2) F-box protein. MAX2 is likely the substrate recognition subunit of a complex involved in proteasome-mediated proteolysis. Different models have been proposed for the role of the SL receptor enzymatic activity[6]. One study demonstrated an interaction between the rice D14 SL receptor and the unique rice DELLA, SLENDER RICE1 (SLR1) that is dependent upon both SL and the hydrolytic activity of D14[9]. D14 crystallization showed that the D-OH reaction product is trapped in the binding pocket, but far from the catalytic triad, forming an altered surface without large structural differences between the apo-D14 and the D14 D-OH complex[9]. In an alternative model, based on co-crystallization and ligand soaking, it was proposed[8,10] that the D-ring is maintained close to the catalytic triad at the bottom of the binding pocket with the ABC tricycle also retained in the pocket.

We characterized the enzymatic activity of the pea RMS3 SL receptor using bioactive, enzyme-activated fluorescent probes and compared it to that of the *Arabidopsis* AtD14 SL receptor. This comparison allowed the investigation of possible specificities between the mycotrophic garden pea, with four natural SLs identified to date, and *Arabidopsis*, a non-host plant for arbuscular mycorrhizal (AM) fungi and in which the presence of canonical SL with the ABC rings is discussed[11,12]. Here we propose a model of SL-reception where the

D-ring product of the RMS3 single-turnover enzymatic activity is covalently bound to the histidine of the catalytic triad, which seems necessary for SL bioactivity.

Results

RMS3 is the pea ortholog of the D14 SL receptor

Five independent allelic *rms3* branching mutants have been isolated in pea (**Supplementary Results**, **Supplementary Fig. 1a-c**). For two of these *rms3* mutant lines, levels of SL from root exudates revealed WT levels of SL production, indicating that SL biosynthesis was not affected (**Supplementary Fig. 1d**). Whereas the synthetic SL (±)-GR24 inhibited branching in the SL deficient *rms1-10* biosynthetic mutant (*Psccd8*), (±)-GR24 treatment did not inhibit branching in the five *rms3* lines (**Supplementary Fig. 1e**), confirming that *RMS3* is involved in SL signaling[13]. We hypothesized that *RMS3* corresponded to *PsD14*, the pea ortholog of the rice gene *D14* encoding the SL receptor[14]. Phylogenic analysis showed that the predicted 267-amino acid PsD14 protein is clearly related to the D14-clade (**Supplementary Fig. 2, Supplementary Table 1**). *PsD14* was sequenced and mutations were found in the *PsD14* gene of each *rms3* mutant. In the *rms3-5* mutant, the Ser within the catalytic triad (position 96) was replaced by Phe. For *rms3-3* and *rms3-4*, Gly/Asp substitutions at position 15 and 28, respectively, likely destabilized the protein, as suggested by differences in free energies between WT and mutant proteins (**Supplementary Fig. 1f**, **3a**; **Supplementary Table 2**). In the *rms3-2* mutant line, a point mutation at the exon-intron junction led to non-splicing of the intron (**Supplementary Fig. 3b)** and to a truncated protein after amino acid 124. Branching phenotypes of the *rms3* pea mutants[15,16] and the identification of mutations in the *PsD14* sequence from all five independent *rms3* mutant alleles, strongly support the conclusion that *RMS3* is *PsD14*.

We next compared the predicted RMS3 protein structure with AtD14 and a paralog of AtD14, HYPOSENSITIVE TO LIGHT (AtHTL)[17] (also known as KARRIKIN INSENSITIVE2 (AtKAI2)). AtHTLis required for karrikin signaling. Karrikins, found in the smoke of burning vegetation[16,18,19], stimulate seed germination, and photomorphogenesis by repressing hypocotyl elongation[16]. Protein alignment of the D14 homologs revealed a potential RMS3 catalytic triad (Ser96, Asp218, and His247), and six conserved hydrophobic phenylalanine residues surrounding the entrance to the ligand-binding pocket (**Supplementary Fig. 4**).

RMS3 can interact and hydrolyze SLs

Interactions between RMS3 and SL analogs were assessed using differential scanning fluorimetry (DSF) and intrinsic fluorescence for estimating apparent dissociation coefficients (K_d). Using DSF, a shift in RMS3 melting temperature was observed with all tested bioactive SL analogs for shoot branching whereas no shift was observed for the inactive compounds (±)-4'-desmethyl-2'-*epi*-GR24 (lacking a methyl group on the D-ring), ABC tricycle or D-OH (**Supplementary Fig. 5**) suggesting that RMS3 interacts with SLs and that SL-mediated destabilization and bioactivity are highly correlated. The 8 °C decrease in RMS3 melting temperature was consistent with the GR24-mediated destabilization observed in other SL receptors[6,8] (**Fig. 1b, Supplementary Fig. 6**). SL

stereochemistry mediates various biological responses with (+)-GR24 highly active for repressing shoot branching in comparison to (−)-GR24[20]. K_d values varied from 15.7 μM for the highly active analog (+)-GR24, 35.9 μM for (−)-GR24, to 137.1 μM for (±)-solanacol (**Fig. 1a**), which has low bioactivity for shoot branching in pea[21] (**Fig. 1c, Supplementary Fig. 7-8, Table 1**). Interestingly, DSF and intrinsic fluorescence experiments revealed that (±)-4'-desmethyl-2'-*epi*-GR24 and, surprisingly, ABC were able to bind RMS3 without inducing destabilization, as observed for karrikin with AtHTL[22] (**Supplementary Fig. 7**). These results indicated that SL-mediated destabilization is required for bioactivity as suggested for OsD14[8]. (±)-GR24 induced a shift in melting temperature of the $RMS3^{S96C}$ mutant protein, but not of $RMS3^{S96A}$. The estimation of the apparent K_d of (±)-GR24 with $RMS3^{S96C}$ (153.5 μM *vs* 22.0 μM with RMS3) (**Supplementary Fig. 7, Table 1**) indicated that modification of the nucleophilic residue of the triad did not suppress SL binding to the receptor, but strongly decreased the affinity for (±)-GR24. This decrease resulted from the low affinity of $RMS3^{S96C}$ for (−)-GR24 but not for (+)-GR24 (675.6 μM *vs* 15.7 μM) (**Supplementary Fig. 8**).

We characterized the hydrolysis activity of RMS3 by incubating (±)-GR24 with RMS3, followed by ultra-performance liquid chromatography-tandem mass spectrometry (UPLC-MS) analysis. We observed products corresponding to the ABC tricycle, and a compound of 270 $gmol^{-1}$ (**Fig. 1d**). The ABC fragment was observed at varying levels when either enantiomer of GR24 or the epimer (±)-2'-*epi*-GR24 were incubated with RMS3, (**Fig. 1e-f**). The second product of 270 $gmol^{-1}$ was observed with (+)−, (−)-GR24[6,8] and (±)-2'-*epi*-GR24, and we suspected this is the result of hydrolysis of a by-product of the GR24 synthesis. Indeed none of the MW 270 compound was detected after a new experiment performed with (±)-GR24 purified by preparative HPLC (**Supplementary Figure 9**). RMS3 was therefore able to hydrolyze the different GR24 enantiomers and epimers but the absolute configuration influenced the level of hydrolysis **(Fig. 1d-e).** The $RMS3^{S96A}$ and $RMS3^{H247A}$ mutant proteins, where key residues of the catalytic triad were replaced, failed to hydrolyze GR24, whereas the more conservative $RMS3^{S96C}$ mutation retained limited hydrolase activity (**Fig. 1d-e, Supplementary Fig. 9**).

In order to compare hydrolysis kinetics of D14 homologs we first incubated the generic esterase reporter *p*-nitrophenyl acetate (*p*-NPA) with RMS3, AtD14 and AtHTL. All showed a Michaelis-Menten kinetics, but with very low efficiency compared with the well known active hydrolase AtMES9 (METHYL ESTERASE 9)[23]. In comparison to $RMS3^{S96A}$, the $RMS3^{S96C}$ mutant protein still exhibited hydrolysis activity, with a similar efficiency as the *Arabidopsis* AtD14 SL receptor when using *p*-NPA (**Supplementary Fig. 10, Supplementary Table 3**) indicating that this mutation did not suppress enzymatic activity.

Design of bioactive profluorescent probes

To further investigate the hydrolysis kinetics of SL-receptors, we synthesized profluorescent molecular probes that have SL-like bioactivity for shoot branching. Probe design was based on the hydrolysis of the synthetic SL GR24 by the RMS3 SL receptor, which leads to the formation of the ABC tricycle and D-OH derivatives. Previous studies have shown: 1) that replacement of the SL ABC tricycle with a simple aromatic ring led to highly bioactive SL

analogs, and 2) substitutions on the D-ring (at 4' positions) dramatically influenced bioactivity[21,24].

Phenol fluorophores are quenched when engaged in a covalent bond[25]. When hydrolyzed, the fluorophore is released and fluorescence is dramatically enhanced, thereby providing a readout of the SL receptor hydrolytic activity. Several probes with varying D-ring structures were designed using the 6,8-difluoro-7-hydroxy-4-methylcoumarin[26] (DiFMU) fluorophore to mimic the ABC tricycle of SLs (**Fig. 2a**). (±)-GC240 had the canonical D-ring structure (present in natural SLs) with one methyl group at 4' position; (±)-GC486 had no methyl group (as the non-active (±)-4'-desmethyl-2'-*epi*-GR24) whereas (±)-GC242 had 2 methyl groups (as the highly active (±)-3'-Me-GR24 (**Fig. 2a**). Both enantiomers (+)- and (−)-GC242 were separated by chiral chromatography from the racemic mixture (**Supplementary Fig. 11a-c**). Their absolute configurations were determined by single crystal X-ray diffraction (**Supplementary Fig. 11d**).

Only (±)-GC486 was inactive for shoot branching in pea even when directly applied to the axillary bud at 5 μM (**Supplementary Fig. 12a**). (±)-GC242 was active on the SL-deficient *rms1* mutant, but not on the *rms3-5* signaling mutant (**Fig. 2b**) and showed higher activity than (±)-GR24 and (±)-GC240, likely because of its higher stability (**Supplementary Fig. 12a,c**). These results suggested that (±)-GC242 was a specific bioactive SL mimic that can repress axillary bud outgrowth via RMS3. The bioassay for shoot branching in pea revealed a similar bioactivity for (+)- and (−)-GC242 enantiomers at high concentrations (1 μM) (**Fig. 2c**). At lower concentrations (1–0.1 nM), only (−)-GC242, which has the same absolute stereochemistry (*R*) at the C2' position as natural SLs, was bioactive.

In *Arabidopsis*, (±)-GC242 (1 μM) repressed shoot branching of the SL deficient mutant *max4-1* as well as (±)-GR24 (**Fig. 2d**). Bioactivity of the probes was also tested on hypocotyl elongation. In *Arabidopsis*, (±)-GR24 and KAR inhibit hypocotyl growth via AtD14 and HTL[16]. For hypocotyl growth, (±)-GR24 suppressed hypocotyl elongation in WT, *Atd14-1* and *htl-3* single mutant seedlings, but not in the *max2-1* mutant or *Atd14-1 htl-3* double mutant. Thus, we confirmed that (±)-GR24 represses hypocotyl elongation via AtMAX2 and redundantly *via* AtD14 and AtHTL (**Fig. 2e**). Similar results were obtained for (±)-GC242, except that no effect was observed on the *Atd14-1* mutant, suggesting that (±)-GC242 inhibits hypocotyl elongation primarily *via* AtD14 and AtMAX2. Interestingly, the *Atd14-1 htl-3* double mutant treated with (±)-GC242 showed longer hypocotyls (**Fig. 2e**). Similarly (±)-GC240 repressed hypocotyl elongation in *htl-3* in contrast to (±)-GC486 and a slight increase in hypocotyl growth was observed on *max2-1* (**Supplementary Fig. 12d**). This increase, still not understood, is reminiscent to what is observed in the analysis of SL response in the *rms4/Psmax2* pea mutant[27]. Together these data demonstrated SL-like bioactivity of the profluorescent probes acting via the SL receptor.

RMS3 enzymatic activity is required for bioactivity

Interactions between the probes and RMS3 were monitored by DSF and intrinsic fluorescence. (±)-GC242 (**Fig. 2f**), its two enantiomers, and (±)-GC240 induced a clear shift in melting temperature of the RMS3 protein whereas no destabilization of the mutant protein

RMS3^{S96A} was observed. (±)-GC242 also destabilized the RMS3^{S96C} mutant protein. (±)-GC486 induced destabilization of RMS3 only at very high concentrations (**Supplementary Fig. 13**). The apparent K_d fell to the same extent for all these probes ((±)-GC242, (±)-GC240, (±)-GC486) differing only in their D-ring structure, indicating that the ABC rings alone, which vary among natural SLs, influence the affinity to the receptor (**Fig. 2g, Supplementary Fig. 13-14, Table 1**). DiFMU alone induced a small stabilization (**Supplementary Fig. 13i**) suggesting an interaction with RMS3, confirmed by intrinsic fluorescence. The DiFMU can bind RMS3 with a stronger affinity than ABC (K_d = 20 μM *vs* K_d = 271 μM) (**Supplementary Fig. 14e**).

We confirmed that RMS3 can hydrolyze (±)-GC242 by LC-MS analysis and observed free DiFMU fluorophore (**Supplementary Fig. 15**). We obtained similar results to those seen with (±)-GR24 when the substrate was incubated with the mutant proteins (**Supplementary Fig. 15**). The higher bioactivity and stability of (±)-GC242 compared to (±)-GC240 led us to use (±)-GC242 for further studies (**Supplementary Fig. 12a,c**).

We examined the kinetics of RMS3 hydrolytic activity by monitoring DiFMU fluorescence. A biphasic time-course of fluorescence was observed, consisting of a burst phase (corresponding to the pre-steady state) followed by a plateau phase that was reached within 5 min (**Fig. 3a**). The substrate:product ((±)-GC242:DiFMU) stoichiometry was not 1:1 (**Fig. 3a**), suggesting that the enzyme was potentially inhibited by the products of the enzymatic reaction tightly bound to RMS3. In contrast with the non-specific substrate *p*-NPA, no steady state was observed during (±)-GC242 hydrolysis in the range of substrate concentrations tested (**Supplementary Fig. 10**), indicating that the (±)-GC242 hydrolysis by RMS3 doesn't follow a Michaelis-Menten kinetic. The quick onset of the plateau without increase of product with further incubation time, suggest that RMS3 could act as single turnover enzyme.

As expected, mutating the serine or histidine of the catalytic triad to alanine blocked (±)-GC242 hydrolysis, and the RMS3^{S96C} mutant exhibited a dramatic decrease in hydrolytic activity (**Fig. 3a**). In order to confirm the *in vitro* data obtained with RMS3 mutant proteins, we used the *Arabidopsis* AtD14 mutant proteins to perform complementation experiments in *Arabidopsis*. The different mutant proteins including AtD14^{S97C} failed to complement the branching phenotype of *Atd14-1*. Only a small but significant decrease in branching was observed after (±)-GR24 (1 μM) application in one AtD14^{S97C} transformant indicating that the mutant protein could perceive exogenous (±)-GR24 *in planta* but not the endogenous SLs and that an efficient SL hydrolysis is required for the perception of endogenous SLs (**Fig. 3b-c, Supplementary Fig. 16**). No fluorescence was detected using AtHTL (**Fig. 3d**), even though it showed an esterase activity on *p*-NPA. This suggested that AtHTL may not hydrolyze the probe, as suggested by the response of the *htl-3* mutant to (±)-GC242 (**Supplementary Fig. 12d**).

Given that our kinetic assays with (±)-GC242 did not reflect classical Michaelis-Menten parameters, we defined k_{cat} as the rate constant of the pre-steady-state phase, and $K_{1/2}$ as the probe concentration that gives half maximal velocity (V_{max}) (**Fig. 3e**). RMS3 and AtD14 exhibited similar parameters with a slight difference in the affinities ($K_{1/2}$ = 0.49 μM and

1.19 μM, respectively). The higher $K_{1/2}$ value of RMS3 for (+)-GC242 compared with (−)-GC242 (17.42 and 1.56 μM, respectively), confirmed the influence of stereochemistry on the hydrolytic activity, also shown by the bioassay (**Supplementary Fig. 12**). Comparison of (±)-GC242 and (±)-GC240 hydrolysis showed that the C3' methyl chain had only a minor influence on the enzymatic constants (**Table 1, Supplementary Fig. 17**).

We dissected the enzymatic properties of (±)-GC242 hydrolysis by RMS3, by testing increasing amounts of RMS3 protein in a constant (±)-GC242 concentration. The height of the plateau was dependent on the concentration of the enzyme rather than the substrate. This suggested that the enzyme was the limiting reagent and could not hydrolyze the remaining substrate (**Fig. 4a**). This also suggested that the enzyme was being inactivated following the hydrolysis of one SL molecule, as the product:substrate ratio was not 1:1. Reciprocally, when increasing concentrations of (±)-GC242 were added to a constant amount of RMS3 protein, the height of the plateau reached a maximum value when the substrate:protein ratio exceeded 1 (**Fig. 4b**). This maximum was not observed when *p*-NPA was used as a substrate (**Supplementary Fig. 10a),** highlighting the specificity of the interaction between our probe and the enzyme. To further confirm this irreversible inhibition, two successive additions of RMS3 were performed. After the reaction reached a plateau, adding RMS3 led to another rapid increase in fluorescence (**Fig. 4c**), confirming that the first plateau did not result from limited substrate, but from RMS3 inactivation. These results suggested that RMS3 act as a single turnover enzyme and could form a stable intermediate with one of the products of the hydrolysis reaction, probably the D-ring, according to the release of the DiFMU observed in our enzymatic assay and the mechanism previously proposed in rice[10].

A RMS3-D-ring complex appears essential for bioactivity

Monitoring fluorescence with other probes showed that they were all hydrolyzed by RMS3 (**Fig. 4d**). The (±)-GC486 probe showed a fluorescence burst that was too rapid to estimate the kinetic constants without a stopped-flow system. Remarkably, the fluorescence emitted with (±)-GC486 (1 μM) was very high compared to that with all other probes and the product:substrate stoichiometry was 1:1. This suggested that this inactive compound can be hydrolyzed by RMS3 but that it did not inhibit the enzyme (**Fig. 4d**). Furthermore, the conserved methyl on the D-ring may be essential for the irreversible inhibition of RMS3.

Surprisingly the stoichiometry RMS3: DiFMU in the fluorescence traces (**Fig. 4c-d**) did not reach 1:1, as expected from our hypothesis of single turnover. It is possible that our enzyme preparation would not be 100% active. Moreover, the leaving group may also perform a product inhibition as suggested by the ability of the DiFMU and the ABC tricycle to bind RMS3 (**Supplementary Fig.7g, 7i, 13i, 14e**). The DiFMU molecules released in the medium could be partly trapped in the binding pocket of the apo-protein, and consequently could inhibit the emission of fluorescence by these proteins. To test this hypothesis, a competition assay was performed by adding increasing amounts of (±)-ABC tricycle to the reaction mixture. A modification of the $K_{1/2}$ without change of the V_{max} was observed (**Fig. 4e**) confirming that (±)-ABC tricycle acted as a competitive inhibitor (K_i = 28.8 μM) (**Fig. 4e, Table 1, Supplementary Fig.18a**).

To investigate whether SL analogs were acting similarly as (±)-ABC tricycle, competition assays were performed with different SLs. (±)-GR24 was also able to inhibit (±)-GC242 hydrolysis. It seems to modify $K_{1/2}$ and V_{max}, and so could act as an irreversible competitive inhibitor. A constant of inactivation of K_i = 0.102 μM was estimated for (±)-GR24 (**Fig. 4f, Table 1, Supplementary Fig.18b**). As expected from previous studies[21], (+)-GR24 was the strongest inhibitor (K_i = 0.07 μM) with (±)-2'-*epi*-GR24 (K_i = 0.23 μM), whereas (−)-GR24 (K_i = 5.17 μM) or (±)-solanacol (K_i = 21.5 μM) were poor inhibitors. This confirmed the high stereospecificity of SL receptors (**Supplementary Fig. 19, Table 1**)[20].

The difference in competition mechanisms between ABC and (±)-GR24 suggested a key role for the D-ring in determining the mode of inhibition. We therefore investigated whether the D-ring interacted with RMS3. (±)-GR24 was incubated with RMS3 at pH 6.8 and mass-spectrometry analysis was performed in native and denaturing conditions. A mass shift corresponding to the D-ring covalently bound to the protein was detected in both conditions (**Fig. 5a**). The localization of the D-ring attachment was determined by digestion of the RMS3-D-ring complex obtained from incubating RMS3 with (±)-GR24 or (±)-GC242. Peptides corresponding to the amino acids 246–262 of RMS3 plus the D-ring with both substrates were found (**Fig. 5b, Supplementary Fig. 20**). The D-ring was specifically attached to His 247 of the catalytic triad (**Supplementary Fig. 21-22, Supplementary Table 4**) with a ratio of modified RMS3-complex/RMS3 of 91/9 after 5 min of incubation with (±)-GC242 (**Supplementary Fig. 22a**). No complex formation was detected with the $RMS3^{H247A}$ mutant protein (**Supplementary Fig. 23a-c)** and a low amount of complex with the $RMS3^{S96C}$ mutant protein was identified in accordance with the previous hydrolysis data (**Supplementary Fig. 23d-f**). The modification also occurred after incubation of the *Arabidopsis* AtD14 protein with (±)-GC242 (**Supplementary Fig. 23g-i**). The D-ring attached to His 247 was not found when RMS3 was incubated with (±)-GC486 (**Supplementary Fig. 20b**). Consequently, a non-methylated D-ring cannot be covalently linked to the His 247. Instead it is released together with the DiFMU, liberating the enzyme for another hydrolysis reaction. The stability of the RMS3-D complex was demonstrated at pH 5.2 and pH 7.7 (**Supplementary Fig. 24**).

Discussion

During evolution, α/β-hydrolases SL receptors of vascular plants, have conserved the Ser, Asp, His catalytic triad and hydrolyze SLs. We showed that the enzymatic reaction performed by the SL receptor generated its own D-ring ligand covalently bound to the His of the catalytic triad, that remained trapped inside the protein. This binding appeared to be essential for SL bioactivity.

Co-crystallization of rice OsD14 and GR24 confirmed that the serine 96 residue creates a nucleophile attack at SL C5' position[10]. The hydrolysis induces the formation of an aldehyde intermediate bound to the serine, and departure of the ABC tricycle from the enzyme. Profluorescent probes allowed us to quantify the production of this leaving group, revealing that RMS3 acted as single turnover enzyme as shown by the biphasic kinetic due to the formation of a covalent intermediate. In addition it seemed that the leaving group, at least *in vitro,* was able to bind the SL receptor and to induce a product inhibition. These two

phenomena can explain the low hydrolysis rate observed in previous reports[6] (**Fig. 3**). The ability of the leaving group to exit the enzyme was quantified by the k_{cat}, and is probably controlled by the intrinsic pKa of the ABC tricycle[7] (**Supplementary Fig. 5**). The design of various probes with different D-rings indicated that the methyl in 4' position, conserved in all natural SLs, is essential for the formation of the covalent complex between His 247 and the D-ring[28], (**Fig. 5a-b, Supplementary Table 4**). These results suggested a second nucleophile attack, in which the nitrogen atom of the imidazole group attacks the aldehyde intermediate at the C2' position to form a covalent bond with the D-ring **(Supplementary Fig. 25)**.

All these results led us to propose a kinetic mechanism in which SL binds and is hydrolyzed by the receptor, forming a stable intermediate with the D-ring covalently bound to the catalytic histidine and releasing the ABC tricycle. This covalent intermediate may induce destabilization, conformational change, or surface change to recruit binding partners (**Fig. 5c**). Whether and how the covalent binding of the D-ring to the His results in the interaction with the F-box protein needs further research. This mechanism of hormone perception, which involves a suicide-like reaction, may explain the rapid, AtMAX2-dependent degradation of AtD14 that is observed after SL treatment[29].

In agreement with the DSF and intrinsic fluorescence assay results, no bioactivity was observed for the D-ring itself for shoot branching in pea[21]. The D-ring may have to be bound to an hydrophobic group to be an active SL, the hydrophobic ABC tricycle acting as a cargo to bring the D-ring to the catalytic triad (see logP values in **Supplementary Fig. 5**). The ABC rings may interact with the six phenylalanine residues that line the active-site gorge of the D14 structure (**Supplementary Fig. 4**) as suggested by the decrease in binding activity observed with the $OsD14^{F126V}$ mutant protein[8]. A potential product inhibition by the released ABC may interfere according the relative values of the constant K_i and $K_{1/2}$ (**Fig. 5c**) and may be considered in future research.

SL perception evolved multiple times in different organisms including parasitic plants and arbuscular mycorrhizal fungi[30,31]. Basal land plants are able to synthetize and to respond to SLs but do not possess canonical D14 SL receptor[32]. It is proposed that SL perception evolved through gene duplication and neofunctionalization of HTL/KAI2 paralogs. In obligate parasitic plants of the Orobanchaceae, an increase in HTL/KAI2 gene copy number is observed [31,33]. All proteins have the conserved catalytic triad and profluorescent agonists were designed for SL receptor identification and for the dynamic *in vivo* observation of SL signaling mediating seed germination. Bioactive profluorescent agonists should continue to represent powerful tools[7] for a better understanding of SL perception and its evolution.

ONLINE METHODS

Plant material and growth conditions

Pea (*Pisum sativum*) branching mutant plants used in this study were derived from various cultivars of pea after ethyl methanesulfonate (EMS) mutagenesis and were described previously[15,34-36]. The *rms1-10* (M3T-884), *rms3-4* (T2-30) and *rms3-5* (M2T-32) mutants were obtained from the dwarf cv Térèse. The *rms3-1* (K487) and *rms3-2* (K564) mutants

were obtained from the tall line Torsdag and the *rms3-3* mutant (WL6042) from the dwarf cv Raman. All five *rms3* mutations are recessive and allelic. Plants were grown in a greenhouse under long days as described[37]. For longer culture, one plant per 2-L pot was grown.

All *Arabidopsis thaliana* plants used in this study originated from the Columbia (Col-0) ecotype background and have been described previously: *max4-1*[38] *Atd14-1, max2-1*[39], and *htl-3*, *Atd14-1 htl-3*[40]. The *max2-1* and *max4-1* mutants were kindly provided by P. Brewer (University of Queensland, Australia), *Atd14-1* mutant by M. Waters (University of Western Australia, Australia) and *htl-3*, *htl-3 Atd14-1* by P. McCourt (University of Toronto, Canada). Plants were grown in a growth room under long-day conditions (16 h light/8 h dark). For the experiment described in **Figure 2e** and **Supplementary Figure 12d**, seeds were sown onto solid agar (0.8%, w/v) in Petri dishes and stratified at 4°C in darkness for 48 h, then transferred to white light (120 μmol m^{-2} s^{-1}). Seedlings were grown for 5 or 6 days and were transplanted to individual plastic pots (0.2 L) with a 1:1:1 vermiculite:perlite:peat mixture and grown in a glasshouse under natural light, until they were 48 days old. The greenhouse experiments were carried out in spring, under long photoperiods (15–16 h per day); daily temperatures fluctuated between 18°C and 25°C. Peak levels of PAR were between 700 and 1000 μmol m^{-2} s^{-1}. Plants were watered twice a week with tap water.

Isolation of *PsD14* gene—To obtain the pea homolog of the rice Os*D14*, degenerate primers PsD14_138F and PsD14_701R were designed from a protein alignment between *D14* homologs from *Arabidopsis* (GeneBank AEE74023.1), rice (GeneBank AK070827), Medicago EST (TC118743) and *Glycine max* (GeneBank AK245636). A fragment of 665 bp was amplified. The 5' region was obtained by PCR walking with three specific primers, RMS3_170R, RMS3_160R and RMS3_150R, and the restriction enzyme *Dra*I (Fermentas). The 3'sequence of *RMS3* was obtained by 3'RACE PCR on pea cDNA with gene-specific nested primers RMS3_741F and RMS3_788F.

Identification of *rms3* mutations—The *PsD14* gene was amplified with RMS3_1F and RMS3_1312R primers from genomic DNA in the *rms3-1* to *rms3-5* mutants and their corresponding WT parental lines to search for point mutations associated with the phenotype of *rms3* mutants. For the analysis of the non-splicing of the intron in the *rms3-2* mutant, a PCR was performed on leaf cDNA from Torsdag and *rms3-2* with water (H_2O) and genomic DNA (gDNA) as controls. The primer pair RMS3_142F and RMS3_579R surrounded the intron.

SL Sampling and analysis[37]—Pea plants were germinated in vermiculite for 6 d and then transferred to aerated hydroponic complete nutrient solution culture, with 12 plants in 6 L of solution in a growth cabinet set at 23 °C, 55% relative humidity during the day and 15 °C, 65% relative humidity at night, with a 16-h photoperiod and light intensity of 300 μmol m^{-2} s^{-1} provided by cool-white fluorescent lamps supplemented with tungsten lamps. At 19 d after germination, the solution was replaced with water, then 24 h later, batches of 12 plants were transferred to 900 mL of water into which exudate was collected for 24 h. Deuterium-labeled SL internal standard (20 ng of d1-fabacyl acetate; a generous gift of Koichi Yoneyama) were added to each sample. Fabacyl acetate was extracted with 0.6

volume of ethyl acetate, followed by back-extraction with 0.1 M KH_2PO_4. The ethyl acetate fraction was dried with anhydrous $MgSO_4$, filtered, and evaporated to dryness at 35 °C. Samples were redissolved in dry acetone, transferred to autosampler vials, redried, dissolved in acetonitrile:water (30:70, v/v), and filtered (0.45 μm) prior to analysis by liquid chromatography-mass spectrometry multiple reaction monitoring (MRM) in positive ion electrospray mode using the Agilent 1100 LC System and an Applied Biosystems Sciex QTrap mass spectrometer. The column was Phenomenex 3 μm C18 Luna 100 × 2 mm, heated to 40 °C with a flow rate of 200 μL min^{-1}. The initial mobile phase was 45.5% acetonitrile in 0.1% aqueous formic acid. After 1 min, a linear gradient to 77% acetonitrile over 19 min was applied, then increased to 95% acetonitrile for 3 min. Appropriate MRM transitions were monitored for the labeled standard and corresponding unlabeled fabacyl acetate. For the quantitations reported here, the transitions were mass-to-charge ratio 406 to 232 for d1-fabacyl acetate and 405 to 231 for fabacyl acetate. Three biological replicates representing pools of 12 plants were analyzed for each genotype. SL content was calculated from MRM peak areas by the stable isotope ratio method.

Pea shoot branching assay—The compounds to be tested were applied directly to the axillary bud with a micropipette as 10 μL of a solution containing 0.1% acetone with 2% polyethylene glycol 1450, 50% ethanol and 0.4% DMSO[21]. The control-0 is the treatment with 0.1% acetone without compound. 24 plants were sown per treatment in trays (2 repetitions of 12 plants). The treatment was generally done 10 days after sowing, on the axillary bud at node 3. The branches at nodes 1 to 2 were removed to encourage the outgrowth of axillary buds at nodes above. Nodes were numbered acropetally from the first scale leaf as node 1 and cotyledonary node as node 0. Bud growth at node 3 was measured with digital callipers 8 to 10 days after treatment. Plants with damaged main shoot apex or showing a dead white treated-bud were discarded from the analysis. Unless stated, the SL-deficient *rms1-10* pea mutant was used for all experiments.

***Arabidopsis* shoot branching assays—**The SL-deficient *max4-1 Arabidopsis* mutant was used for all experiments. Plants were grown under hydroponics culture conditions in greenhouse. Seeds were surface sterilized for 8 min in a solution of ethanol (95%)-Bayrochlore™ (Bayrol Mundolsheim, France)(10%), and were rinsed twice with ethanol (100%). Each seed was sown on top of a cut Eppendorf tube filled with agar medium containing 0.65% agar. Tubes were soaked in water and stored in dark at 4°C for 2 d. Four plants per pipette tip box (12 × 8 × 6 cm) were grown and supplied with nutrient solution as previously described[24] at a concentration of 5 $mL.L^{-1}$ (540 ml of solution per box). Nutrient solutions were changed every 7 d. At 29 d after sowing, (±)-GR24/(±)-GC242 were applied during 3 weeks and changed every week with the nutrient solution. 20 plants grown in 5 pipette tip boxes were grown and analyzed for each condition by counting the number of rosette axillary shoots per plant.

Arabidopsis* hypocotyl elongation assays—Arabidopsis* seeds were sterilized by 95% ethanol for 10 min, and were plated on half Linsmaier and Skoog (LS) media (Caisson laboratories) containing 0.8% agar, supplemented with indicated concentrations of (±)-GR24 or (±)-GC242 (stock 1000 × in acetone) or with acetone (control). Seeds were stratified at

4 °C (2 days in dark) then transferred in growth chamber at 22 °C, under 20-30 μE /m^2/sec of white light in long day conditions (16 hr light/8 hr dark). Plates were photographed and hypocotyl lengths were quantified using ImageJ (http://imagej.nih.gov/ij/).

Constructs, generation of transgenic lines, and phenotype analysis—The expression vectors for transgenic *Arabidopsis* were constructed by MultiSite Gateway Three-Fragment Vector Construction kit (Invitrogen). All the D14 constructs were tagged with 6xHA epitope tag at their C-terminus. Lines were resistant to hygromycin. Branching phenotype was quantified on 5 week-old plants. AtD14 native promoter (0.8 kb) was amplified by PCR from Col-0 genomic DNA and cloned into *pDONR-P4P1R*, using Gateway recombination (Invitrogen) (see **Supplementary Table 5** for primers). AtD14cds was PCR amplified from Col-0 cDNA and recombined into *pDONR221* (Invitrogen). *6xHA* with a linker (gift from U. Pedmale) was cloned into *pDONR-P2RP3* (Invitrogen). The suitable combination of promoter, Atd14cds and 6xHA was cloned into the *pH7m34GW* final destination vectors by using three fragments recombination system[41], and named pD14::D14-6xHA. Transformation of *Arabidopsis Atd14-1* homozygous mutant was performed according to the conventional dipping method[42], with Agrobacterium strain GV3101. For all constructs, more than 20 independent T1 lines were isolated and between 2 to 4 representative single-insertion lines were selected in T2. Only 2 lines per constructs were shown in these analyses. Phenotypic analysis shown in **Figure 3** and protein extraction shown in **Supplementary Figure 16b** were performed on segregating 48 day-old T2 lines after selection on hygromycin plates (See growth conditions). Branching assay in **Supplementary Figure 16a** was performed on the T3 homozygous lines.

Protein extraction and immunoblotting—Total protein extract was prepared from 100 mg of 40 day-old leaves in Laemmli buffer and boiled for 5 min. Total protein were separated by 4-12% SDS-PAGE and transferred onto polyvinylidene difluoride membrane (Bio-Rad) probed with anti-HA antibody (1:10000; Roche 13800200).

Site-directed mutagenesis—Site-directed mutagenesis experiments were performed using QuickChange II XL Site Directed Mutagenesis kit (Stratagene), performed on pMAD300, pGEX-RMS3 or pD14::D14-6xHA (see **Supplementary Table 5** for primers). Mutagenesis was verified by systematic DNA sequencing.

Cloning, heterologous expression and purification of recombinant proteins—Recombinant protein was expressed in 2 different systems. For mass spectrometry analysis and enzymatic degradation, protein was expressed with a 6xHIS-tag. For DSF assay, enzymatic assay with profluorescent probes and *p*-nitrophenyl ester, and intrinsic fluorescence assay, protein was expressed with a removal GST tag.

Expression and purification of RMS3-HIS and RMS3^{S96A}-HIS protein

Gene cloning—A purified plasmid containing our synthesized gene was purchased from the GeneArt®(Invitrogen). *Nde*I / *EcoR*I fragments with the expected size were gel-purified, digested with *Nde*I/*EcoR*I (New England Biolabs) and ligated into expression vector pET-28a(+) (Novagen, Darmstadt, Germany). The recombinant plasmid pET28-RMS3,

named pMAD300, was then transformed into competent *E. coli* DH5 alpha cells from NEB. The positive clones were identified by restriction enzyme digestion and subjected to plasmid isolation. The fidelity of the inserted fragment into pET-28a(+) vector was confirmed by sequencing on both strands by Eurofins Genomics (Ebersberg, Germany).

Protein expression—The recombinant vector pMAD300, which places the *RMS3/PsD14* gene under the control of a T7 promoter, was transformed into the *E. coli* Rosetta (DE3) from Novagen and induced by IPTG. The induced crude extract containing the hydrolase were analyzed by SDS–PAGE. Recombinant RMS3 was purified to homogeneity from the supernatant of cell lysate by single-step affinity chromatography on a Ni–NTA column. SDS–PAGE of the purified enzyme gave a single band corresponding to a molecular of about 31.7 kDa, which was in accordance with the molecular weight calculated from the amino acid sequence obtained. From 1L of bacterial culture, 20 mg of pure protein were obtained. *E. coli* Rosetta (DE3) cells harboring pMAD300 were grown in a 3 L flask containing 1 L of 2xYT medium with 30 mg/L kanamycin and 34 mg/L chloramphenicol at 37 °C until optical density at 600 nm reached 0.5, then induced with 0.2 mM isopropyl-β-D-thiogalactopyranoside (IPTG). After incubation at 20 °C for 24 h with shaking at 180 rpm, cells were harvested by centrifugation (8000 g, 10 min) at 4 °C and suspended in lysis buffer (200 mM NaCl, 2 mM TCEP, 10% glycerol, 20 mM Tris–HCl, pH 8.0).

Protein purification—The cells were disrupted by sonication, and the supernatant was collected by centrifugation (10 000 g, 30 min) at 4 °C. The supernatant (80 mL) was loaded onto a HisTrap FF Crude column (5 mL, GE Healthcare, Akta Explorer 10S system) pre-equilibrated with Lysis buffer. The column was washed with washing buffer (200 mM NaCl, 2 mM TCEP, 10% glycerol, 25 mM imidazole, 20 mM Tris–HCl, pH 8.0), and protein was eluted with eluting buffer (200 mM NaCl, 2 mM TCEP, 10% glycerol, 100 mM imidazole, 20 mM Tris–HCl, pH 8.0). The fractions containing the 6xHA-tagged RMS3 were collected, concentrated by ultrafiltration on Amicon 10K (5000 rpm, 20 min at 10 °C), dialyzed in phosphate-buffer saline (PBS), 2 mM TCEP, 5% glycerol (3×2 h, 4 °C), then freezed in liquid nitrogen before storage at −80°C. The purified enzyme was used for characterization experiments. The purity and molecular mass of the protein were analyzed by 12% sodium dodecyl sulfate–polyacrylamide gel electrophoresis (SDS–PAGE) under denaturing conditions in Laemmli system[43] (**Supplementary Fig. 26**). The concentrations of proteins in the crude extract were measured according to the Pierce 660 nm protein assay (ThermoScientific) using bovine serum albumin (BSA) as the standard. The protein concentration of the pure enzyme was quantified from the absorbance at 280 nm using Epsilon = 36 758 calculated from amino acids analysis.

The identity of all the purified proteins was verified using matrix-assisted laser desorption/ionization time-of-flight mass spectroscopy (MALDI–TOF MS). For the 6xHIS RMS3 recombinant protein, the mass spectrum shows two peaks at 31,678.1 and 31,856.1 Da after deconvolution. The peak at 31,678.1 Da matches to the theoretical mass of the 6xHIS-RMS3 protein and the peak at 31,856.1 Da corresponds to the same sequence modified by a gluconoylation of the HIS-tag of the protein, a frequent post-translational modification observed in recombinant protein containing an HIStag and expressed in *E. coli*[44]. The

proteolysis confirms the sequence of 283 of the 287 amino acids and the presence of the glucunoylation on the HIS-tag (**Supplementary Fig. 26b**).

Expression and purification of RMS3, RMS3^{S96A}, RMS3^{S96C}, RMS3^{H247A}, AtD14, AtHTL and AtMES9 proteins with cleavable GST tag

Gene cloning—The *RMS3* (residues 1–267), coding sequence from *Pisum sativum,* the *AtD14* (At3g03990) (residues 1–267), the *AtHTL* (At4g37470) (residues 1–269) and the *AtMES9* (At4g37150) (residues 1–256) coding sequences from *Arabidopsis thaliana* were amplified by PCR using adult leaves derived cDNA template and specific primers (see **Supplementary Table 5** for primers) containing a protease cleavage site for tag removal, and subsequently cloned into the pGEXT-4T-3 expression vector. The expression clones was introduced into (*E. coli*) strain BL21-CodonPlus-RIL (Agilent). The expression and purification of RMS3, AtD14, AtKA12, AtMES9 and numerous mutant proteins followed the same method.

Protein expression—The expression clone was introduced into *E. coli* strain BL21-CodonPlus-RIL (Agilent). Cells were grown at 25 °C in Terrific broth (Invitrogen) containing 100 μg/L ampicillin. When the OD_{660} of the cell culture reached ≈ 0.6, isopropyl-β-D-thiogalactopyranoside (IPTG) was added to a concentration of 100 μM to induce expression of the cDNA. Cells were grown at 18°C for an additional 18 h following IPTG induction and then collected by centrifugation at 4000 g for 15 min at 4 °C (Beckman Avanti J-26 XPI) and resuspended in extraction buffer (50 mM Tris–HCl (pH 7.7), 150 mM NaCl and 5 μM β-mercaptoethanol (β-Me)), which included 5% (v/v) glycerol.

Protein purification—After sonication on ice, the lysate was centrifuged at 25,000 × g for 30 min at 4 °C (Beckman Avanti J-26 XPI), and the supernatant was loaded onto a disposable polypropylene column packed with glutathione Sepharose 4B resin (GE Healthcare). The column was washed copiously with extraction buffer. On column, cleavage was performed overnight at 4 °C by adding HRV3C protease, and the target protein was eluted with extraction buffer. The elutated protein was concentrated using an Amicon 10K filter unit (Merck Millipore) to 2 mL and purified by gel filtration using Hi Load 26/60 Superdex 75 prep grade (GE Healthcare) on an AKTA prime system (GE Healthcare) in gel filtration buffer (30 mM Tris, pH 7.7, 50 mM NaCl, 1 mM TCEP). Protein eluted as a sharp single peak with an estimated molecular weight of 30 kD and a purity of >95% as judged by 4-12% SDS/PAGE. Purified protein was concentrated using an Amicon 10K filter unit (Merck Millipore) up to 10 mg/mL with gel filtration buffer. The protein sample was divided into 25-μL aliquots in 0.5-mL tubes (Eppendorf) and immediately frozen in liquid nitrogen. Frozen samples were stored at −80 °C until use. The identity of the purified protein was verified using mass spectrometry (**Supplementary Fig. 27-28**).

Preparations of SL analogues and probes were described in Supplementary Note

Crystallography—Crystals were grown from slow evaporation of a mixture of heptane into acetone solution of the complexes. Data for (−)-GC242 and (+)-GC242 (see **Supplementary Table 6** and **Supplementary Figure 11d**) were collected on a Rigaku Rapid II MM007 HF employing Osmic CMF focusing optics for monochromated Cu-Kα

radiation generated from a rotating anode (λ = 1.54187 Å) according to ω-scan profile data strategy at 293(2) K. Data integration and reduction for were undertaken with CrystalClear_ENREF_52. A multi-scan empirical absorption correction was applied to the data using CrystalClear. Structures were solved using SHELX-S(1997)[45] then refined and extended with SHELX-L(2014)[46]. All non-hydrogen atoms were refined anisotropically whereas hydrogen atoms were located in Fourier differences but refined using a riding model. ORTEP-III_ENREF_54 drawings were made using PLATON_ENREF_56. CCDC 1023160 (**sm**·[(−)-GC242]) and 1023161 (**fm**·[(+)-GC242]) contain the supplementary crystallographic data. Copies can be obtained, free of charge, on application to CCDC, 12 Union Road, Cambridge CB2 1EZ, UK [fax: +44(0) 1223 336033 or deposit@ccdc.cam.ac.uk.]

Chemical stability—(±)-GR24, (±)-GC242 and (±)-GR240 were tested for their chemical stability in an aqueous solution. Aqueous solutions of the compound to be tested (50 μg/mL) were incubated at 21 °C in the HPLC vials. The compounds were first dissolved in DMF (1 mL). Then, 50 μL of the previous solutions were diluted to the final concentration with DMF (450 μL) and PBS (pH 6.8) (500 μL). Indanol (Alfa Aesar, purity > 97.5% (GC)) (25 μL of a 1 mg/mL solution in acetone) as internal standard was added to each solution. The time course of degradation was monitored by UPLC analysis using the system described for the enzymatic degradation of SL analogs and probe. Compounds eluted from the column were detected with a photodiode array detector. The relative quantity of remaining (non-degraded) product was determined by integration comparison with the internal standard.

Physicochemical properties—The LogP, pKa were calculated using the ACD program (https://ilab.acdlabs.com/ilab2/). LogP module provides the estimate of the value of the octanol-water partitioning coefficient for neutral species. Ionization predictor performs fast and accurate calculations of the observed acid-base ionization constants for organic compounds, otherwise known as pK_a, under standard conditions (25 °C and zero ionic strength).

Enzymatic assay with *p*-nitrophenyl esters—Esterase activities against *para*-nitrophenyl acetate (*p*-NPA) (Sigma, purity > 98% (GC area %)), or *para*-nitrophenyl butytate (*p*-NPB) (Sigma, purity ≥98% (TLC)), were determined by measuring the amount of *para*-nitrophenol released by esterase-catalyzed hydrolysis. The *para*-nitrophenyl esters were dissolved in acetonitrile to make a stock solution of 100 mM. The production of *para*-nitrophenol was continuously monitored at 405 nm by use of a Tecan Safire II Plate Reader in 96 well plates. Unless otherwise described, esterase assays were measured with *p*-NPA (0.03 to 4 mM) or *p*-NPB (0.03 to 4 mM) as a substrate in total volumes of 100 μL in 20 mM HEPES, pH 6.8, 200 mM NaCl, 10% glycerol, containing 4% acetonitrile. Unless otherwise described, the final enzyme concentration was 3.33 μM. The assay was carried out at 27°C, and OD_{405} values were measured at 1 min intervals up to 180 or 240 min. All experiments were repeated at least two times with 3 technical replicates. Blank reactions were performed with every measurement under different conditions to subtract the appropriate values for non-enzymatic hydrolysis of substrates from the results. The extinction coefficients of *para*-nitrophenol were also determined under each reaction

condition prior to the measurements. The activity was determined by measuring the initial reaction velocities at various concentrations of *para*-nitrophenyl ester. 3.33 μM of protein were used to measure the initial velocities. K_m, V_{max} and k_{cat} were determined by GraphPad Prism 5 software using nonlinear regression for the Michaelis-Menten equation. For AtD14 and RMS3^{S96C} a linear regression was used to determine the ratio V/K to evaluate the hydrolysis rate.

Enzymatic assay with profluorescent probes—The enzyme assay was determined by measuring the release of fluorescent DiFMU after hydrolysis of profluorescent probes by RMS3, AtD14, AtHTL and rms3 mutant proteins in a Tecan Safire II Plate Reader in a 96-well format. In the assay, to 50 μL profluorescent substrate solution (at varying concentrations, prepared from a 2 mM stock solution in 100% DMSO) in Phosphate buffer saline (PBS) (100 mM Phosphate, pH 6.8, 150 mM NaCl), 50 μL of a solution of protein in same buffer was added simultaneously in all 96 wells using a Integra Viaflo 96 robot. After 45 seconds lag time, the formation of fluorescent DiFMU was recorded with an excitation filter of 355 ± 14 nm and an emission filter of 460 ± 25 nm over 30 min at 20 s intervals at 25°C. During the incubation and in between measurements, the reaction mixture was shaken. Final protein and substrate concentrations are indicated in each figure. All experiments were repeated at least two times with 3 technical replicates. The background reaction rate with no enzyme present was subtracted and the reaction rates were normalized to the reaction rate. The fluorescence of free DiFMU was also determined for each measurements but in absence of enzyme in order to determine the standard curves. The activity was determined by measuring the initial reaction velocities, v_0, at various concentrations of profluorescent probes. 400 nM of protein was used to measure the initial velocities.

The data were analyzed using GraphPad Prism 5 software using non-linear regression. Enzyme initial reaction rate, v_0, at various probes concentrations were fitted to the equation $v_0=\frac{k_{cat}\cdot[E_{tot}]\cdot[S]}{K_{1/2}+[S]}$, where v_0 is the initial reaction velocity, k_{cat} the rate of the slowest step, $E\_(tot)$ the total enzyme concentration, [S] the concentration of the probes, and $K_{1/2}$ is the probes concentration that gives half maximal velocity, in order to determine the single turnover enzymatic constant. In this equation $V_{max} = k_{cat} *[E_{tot}]$. k_{cat} is equivalent to k_2 and $K_{1/2}$ is equivalent to k_{-1}/k_1 in the equation gave in **Figure 5c**.

For the experiment with successive protein additions, 400 nM of protein in 2 μL were added simultaneously in all 96 wells using an Integra Viaflo 96 robot to the previous kinetics and after 45 seconds lag time, the formation of fluorescent DiFMU was recorded again. For competition assay in 96-well format, the initial velocity was determined in the presence of various concentrations of competitor in order to determine the K_i. Before each assay, the competitor was diluted to the 50 μL profluorescent substrate solution to the desired concentrations from 0.1 μM to 100 μM, and measurements were done as described previously. K_i was determined by GraphPad Prism 5 software using nonlinear regression for the Michaelis-Menten equation and a mixed-model inhibition.

Differential Scanning Fluorimetry (DSF)—DSF experiments were performed on a CFX384 Touch™ Real-Time PCR Detection System (Biorad) using excitation and emission wavelengths of 490 and 575 nm, respectively. Sypro Orange ($\lambda_{Ex}/\lambda_{Em}$: 490/610 nm; life technologie) was used as the reporter dye. Samples were heat-denatured using a linear 25 to 95°C gradient at a rate of 1.3 °C per minute after incubation of 25 °C for 30 min in the absence of light. The denaturation curve was obtained using CFX manager software. Final reaction mixtures were prepared in triplicate in 384-well white microplates, and each reaction was carried out in 20-µL scale in Phosphate buffer saline (PBS) (100 mM Phosphate, pH 6.8, 150 mM NaCl) containing 10 µg protein, each concentration of SL derivatives (acetone solution, final acetone concentration was 4%) or profluorescent molecule, (DMSO solution, final DMSO concentration was 4%), and 0.008 µL Sypro Orange. In the control reaction, acetone or DMSO was added instead of chemical solution. The experiments were repeated two times.

Intrinsic tryptophan fluorescence assays and determination of the dissociation constant K_d—Interaction of recombinant proteins with SL analogues and profluorescent probes was monitored by measuring the intrinsic tryptophan fluorescence using a Tecan Safire II Plate Reader in duplicate in a 96-well format. In the assay, to a 50 µL ligand solution (10 different compound concentrations ranging from 0 to 800 µM were prepared from a 2 mM stock solution in 100% DMSO, two additional concentrations were added for $RMS3^{S96C}$) in Phosphate buffer saline (PBS) (100 mM Phosphate, pH 6.8, 150 mM NaCl), 50 µL of a solution of protein in same buffer was added simultaneously in a flat-bottomed, black 96-well plate using a Integra Viaflo 96 robot, to obtain 10 µM final protein concentration. The volume of DMSO in each well was identical. After 30 min. incubation at 25°C, fluorescence was measured. The excitation wavelength at 280 nm was used and an emission spectrum was recorded 5 times over the range of 300 to 400 nm and excitation and emission slit widths of 5 nm. The gain was set to 70, the number of flashes to 50, the flash frequency to 400 Hz, and the integration time to 2 ms.

To quantify the interaction between protein and ligand, the intensities of fluorescence at a fixed wavelength (333 nm) were measured. The degree of saturation ($F(a)$) was determined by transforming the experimental data to the form:

$$F_a = \left| \frac{F_{obs} - F_0}{F_{max} - F_0} \right|$$

where F_0 is the fluorescence intensity in the absence of ligand, F_{obs} is the fluorescence intensity in the presence of non-saturating concentrations of ligand and F_{max} is the fluorescence intensity at saturation. For the K_d determination, the data were fitted by nonlinear regression with hyperbolic function using GraphPad Prism 5.0 software for overall one-site binding. The experiments were repeated at least three times.

Enzymatic degradation of (±)-GR24, (+)-GR24, (–)-GR24, (±)-2'-*epi*-GR24, (±)-GC242 by purified RMS3 protein—The ligand (10 µM) was incubated without and with purified RMS3/$RMS3^{S96A}$/$RMS3^{H247A}$/$RMS3^{S96C}$ (5 µM) for 210 min at 25 ºC in PBS (0.1

mL, pH = 6.8). The solutions were acidified to pH = 1 by addition of trifluoroacetic acid (2 μL) to quench the reaction and centrifugated (12 min, 12,000 tr/min). Thereafter the samples were subjected to RP-UPLC-MS analyses. The instrument used for all the analysis was an Ultra Performance Liquid Chromatography system equipped with a PDA and a Triple Quadrupole mass spectrometer Detector (Acquity UPLC-TQD, Waters, USA). RP-UPLC (HSS C18 column, 1.8 μm, 2.1 mm × 50 mm) with 0.1% formic acid in CH_3CN and 0.1% formic acid in water (aq. FA, 0.1%, v/v, pH 2.8) as eluents [5% CH_3CN, followed by linear gradient from 5 to 100% of CH_3CN (7 min)] at a flow rate of 0.6 mL/min. The detection was performed by PDA and using the TQD mass spectrometer operated in Electrospray ionization positive mode at 3.2 kV capillary voltage.

Direct ESI-MS in denaturant and native conditions—Mass spectrometry measurements were performed with an electrospray Q/TOF mass spectrometer (Q/TOF Premier, Waters) equipped with the Nanomate device (Advion). The HD_A_384 chip (5 μm I.D.nozzle chip, flow rate range 100−500 nL/min) was calibrated before use. For ESI−MS measurements, the Q/TOF instrument was operated in RF quadrupole mode with the TOF data being collected between m/z 400−2990 and 1000-6000 for denaturant and native conditions respectively. Collision energy was set to 10 eV and argon was used as collision gas. Mass spectra acquisition was performed after denaturation of protein (±)-GR24 in 50% acetonitrile and 1% formic acid. In native conditions, mass spectra of RMS3 (50 μM) in 50 mM ammonium acetate in presence or without (±)-GR24 (50 to 500 μM) were acquired with backing and cone voltage set at 4 mBar and 120 V respectively. The Mass Lynx 4.1 software was used for acquisition and data processing. Deconvolution of multiply charged ions was performed by applying the MaxEnt1 algorithm. The protein average masses are annotated in the spectra (**Fig. 5**), and the estimated mass accuracy is ± 2 Da. External calibration was performed with NaI clusters (2 μg/μL, isopropanol/H_2O 50/50, Waters) in the acquisition *m/z* mass range.

Localization of the fixation site of GR24 and GC242 on RMS3—The complexes RMS3 with the ligands were submitted to digestion by a mix LysC/trypsin (Promega Charbonnières les bains France) at pH 7.8 after reduction and alkylation by iodoacetamide or were digested directly after complexation at pH 6.8 by endoproteinase gluC[47]. The coverage was 95.1 % for trypsin and 53.8% for endo proteinase gluC. (Roche Diagnostics, Meylan,France). The digests were desalted on a zip tip C18 (Millipore Saint Quentin en Yvelines France). The peptide were eluted from the ziptip directly by 4 μl of the MALDI matrix solution (5 mg/ml α-Cyano-4-hydroxycinnamic acid in 30% water 70% acetonitrile, 0.1%TFA) and loaded on a MALDI plate. The digests were then analyzed using a MALDI-TOF.TOF mass spectrometer UltrafleXtrem (Bruker Daltonics Wissembourg France). Spectrum between 500 and 4,000 Da were acquired in positive reflectron mode. CID-MSMS spectra were performed with argon as collision gaz. Data were analyzed with Flexanalysis and Biotools (Bruker Daltonics). The Protein digests were also analyzed by nano-Liquid Chromatography (nano-LC) ESI tandem mass spectrometry (MS/MS). These were carried out on a U3000 Dionex nanoflow system connected to an LTQ Orbitrap XL mass spectrometer (Thermo-scientific) equipped with a nanoelectrospray source. The samples were run through a C18 nanocolumn (75 μm i. d. × 50 cm, PepMap100 C18, 3 μm, 100Å;

Dionex) after being injected onto a pre-concentration column with a flow rate of 20 μL/min of 0.1% TFA in water. Peptides were then loaded on the analytical column equilibrated with 0.1% of formic acid in water, elution was carried out by a linear gradient from 2 to 60% of acetonitrile in 60 min at a flow rate of 250 nL/min. The mass spectrometer was operated in data-dependent mode to automatically switch between Orbitrap MS and MS/MS in the linear trap. Tune parameters for the mass spectrometer were set up for all runs: capillary temperature 180 °C, capillary voltage 25 V, tube lens voltage 150 V, and spray voltage 1.5 kV. Survey full scan MS spectra from 450 to 2000 Da were acquired in the Orbitrap set to a resolution R=60,000 at *m/z* 400, after accumulation of 500,000 charges on the linear ion trap. The ions with the most intense signals (up to six, depending on signal intensity, with a trigger threshold at 400) were sequentially isolated for fragmentation in the linear ion trap using CID at a target value of 100,000 charges. The resulting fragments were recorded in the linear trap. MS/MS scans were acquired using an isolation width of 1 *m/z*, an activation time of 30 ms, an activation q of 0.250 and 35% normalized collision energy. Target ions already selected for MS/MS were dynamically excluded for 30 seconds. MS/MS scan event microscan was set up to max ion time of 100 ms and full MS scan event microscan to 200 ms. MS/MS raw files were individually processed through a Proteome Discoverer v1.4 ™ (Thermo -scientific Les Ulis France) workflow and the Sequest search engine was used for localization of peptide in the RMS3 sequence. Peak areas of native and modified peptide were calculated using the MS1 extracted signals of the two exact masses of the ions ± 0.025 Da.

Formation of the RMS3-complex at pH 7.7—RMS3 (40 μM) in solution in ammonium acetate (50 mM, pH 7.7) was incubated for 5 min with (±)-GC242 (400 μM). The mixture was then desalted on ziptip C4 for molecular mass measurement of the complex or digested by LysC/trypsin or endo proteinase gluC.

Stability of the complex at pH 5.2—RMS3 (40 μM) in solution in ammonium acetate (50 mM, pH6.8) was incubated for 5 min with (±)-GC242 (400 μM). The solution was partially evaporated with a vacuum concentrator Speed Vac™ (Thermo scientific). The mixture was incubated in ammonium acetate solution (50 mM, pH 5.2) for 40 minutes. The solution was then desalted on ziptip C4 for molecular mass measurement.

Homology modeling and mutational studies—The homology model of RMS3 was prepared with Phyre2 using the RMS3 sequence against the entire protein data bank. All residues were modeled with >90% confidence[48]. Structural superimpositions and visualizations were created using CCP4mg[49]. The effects of the Glycine mutations on RMS protein stability were analyzed with the SDM server[50].

Phylogenetic analysis—Phylogenic analysis was conducted in MEGA5[51]. Protein sequences were aligned using CLUSTALX. The Maximum Likelihood method based on the Dayhoff matrix based model was used[52]. Initial tree(s) for the heuristic search were obtained automatically as follows. When the number of common sites was < 100 or less than one fourth of the total number of sites, the maximum parsimony method was used; otherwise BIONJ method with MCL distance matrix was used.

Statistical analyses—For testing the normality of distribution, an histogram and the Shapiro-Wilk test were performed (R Commander version 1.7-3). For normally distributed data, a Bartlett's test was performed to compare the variance of samples. Because strong deviations from normality were observed for axillary bud length after SL treatment, the Kruskal-Wallis test was used (R Commander version 1.7-3)[53] and sample size was similar to the one used previously[21]. In other cases, Student's *t*-tests were used. Results from previous experiments were used to have an estimation of SD and GR24 effect on a given character. Minimum sample size was estimated for alpha = 0.05 and power = 0.80.

Supplementary Material

Refer to Web version on PubMed Central for supplementary material.

Acknowledgments

We thank Romain Novaretti from Institut Jean-Pierre Bourgin in Versailles for plant bioassays, Albert Eddie Stewart for helpful discussion, Shane Ken Lin for technical assistance, Jean-Pierre Andrieu, from the IBS platform of the Partnership for Structural Biology and the Institut de Biologie Structurale in Grenoble (PSB/IBS), for the assistance and access to Amino Acids determination facility and Ullas Pedmale for technical advice. We thank Björn C. Willige, Clara Bourbousse, Jesse Woodson, Ullas Pedmale, Adam Seluzicki and David O'Keefe for their comments on the manuscript. We are grateful to the Institut National de la Recherche Agronomique (INRA), the Agence Nationale de la Recherche (contract ANR-12-BSV6-004-01) and the Stream COST Action FA1206 for financial support. A.dS.G and J.C. were partially supported by a grant to J.C. from the National Institutes of Health (RO1 GM094428). J.C. is an investigator of the Howard Hughes Medical Institute. A.dS.G was partially supported by a grant from Catharina Foundation to the Salk Institute. The IJPB benefits from the support of the Labex Saclay Plant Sciences-SPS (ANR-10-LABX-0040-SPS).

References

1. Xie X, Yoneyama K, Yoneyama K. VanAlfen NK, Bruening G, Leach JE. Annu. Rev. Phytopathol. 2010; 48:93–117. [PubMed: 20687831]
2. Gomez-Roldan V, et al. Strigolactone inhibition of shoot branching. Nature. 2008; 455:189–194. [PubMed: 18690209]
3. Umehara M, et al. Inhibition of shoot branching by new terpenoid plant hormones. Nature. 2008; 455:195–200. [PubMed: 18690207]
4. Brewer PB, Koltai H, Beveridge CA. Diverse Roles of Strigolactones in Plant Development. Mol. Plant. 2013; 6:18–28. [PubMed: 23155045]
5. de Saint Germain A, Bonhomme S, Boyer F-D, Rameau C. Novel insights into strigolactone distribution and signalling. Curr. Opin. Plant Biol. 2013; 16:583–589. [PubMed: 23830996]
6. Hamiaux C, et al. DAD2 Is an alpha/beta Hydrolase Likely to Be Involved in the Perception of the Plant Branching Hormone, Strigolactone. Curr. Biol. 2012; 22:2032–2036. [PubMed: 22959345]
7. Tsuchiya Y, et al. Probing strigolactone receptors in *Striga hermonthica* with fluorescence. Science. 2015; 349:864–868. [PubMed: 26293962]
8. Zhao L-H, et al. Destabilization of strigolactone receptor DWARF14 by binding of ligand and E3-ligase signaling effector DWARF3. Cell Res. 2015; 25:1219–1236. [PubMed: 26470846]
9. Nakamura H, et al. Molecular mechanism of strigolactone perception by DWARF14. Nat Commun. 2013; 4:2613. [PubMed: 24131983]
10. Zhao LH, et al. Crystal structures of two phytohormone signal-transducing alpha/beta hydrolases: karrikin-signaling KAI2 and strigolactone-signaling DWARF14. Cell Res. 2013; 23:436–439. [PubMed: 23381136]
11. Abe S, et al. Carlactone is converted to carlactonoic acid by MAX1 in *Arabidopsis* and its methyl ester can directly interact with AtD14 in vitro. Proc. Natl. Acad. Sci. U S A. 2014; 111:18084–18089. [PubMed: 25425668]

12. Wallner E-S, López-Salmerón V, Greb T. Strigolactone versus gibberellin signaling: reemerging concepts? Planta. 2016:1–12.
13. Beveridge CA, Dun EA, Rameau C. Pea Has Its Tendrils in Branching Discoveries Spanning a Century from Auxin to Strigolactones. Plant Physiol. 2009; 151:985–990. [PubMed: 19767387]
14. Alves-Carvalho S, et al. Full-length de novo assembly of RNA-seq data in pea (Pisum sativum L.) provides a gene expression atlas and gives insights into root nodulation in this species. Plant J. 2015; 84:1–19. [PubMed: 26296678]
15. Beveridge CA, Ross JJ, Murfet IC. Branching in pea - Action of genes *Rms3* and *Rms4*. Plant Physiol. 1996; 110:859–865. [PubMed: 12226224]
16. Waters MT, et al. Specialisation within the DWARF14 protein family confers distinct responses to karrikins and strigolactones in *Arabidopsis*. Development. 2012; 139:1285–1295. [PubMed: 22357928]
17. Sun X-D, Ni M. HYPOSENSITIVE TO LIGHT, an Alpha/Beta Fold Protein, Acts Downstream of ELONGATED HYPOCOTYL 5 to Regulate Seedling De-Etiolation. Mol. Plant. 2011; 4:116–126. [PubMed: 20864454]
18. Nelson DC, et al. F-box protein MAX2 has dual roles in karrikin and strigolactone signaling in *Arabidopsis thaliana*. Proc. Natl. Acad. Sci. U S A. 2011; 108:8897–8902. [PubMed: 21555559]
19. Guo Y, Zheng Z, La Clair JJ, Chory J, Noel JP. Smoke-derived karrikin perception by the alpha/beta-hydrolase KAI2 from *Arabidopsis*. Proc. Natl. Acad. Sci. U S A. 2013; 110:8284–8289. [PubMed: 23613584]
20. Scaffidi A, et al. Strigolactone Hormones and Their Stereoisomers Signal through Two Related Receptor Proteins to Induce Different Physiological Responses in Arabidopsis. Plant Physiol. 2014; 165:1221–1232. [PubMed: 24808100]
21. Boyer F-D, et al. Structure-Activity Relationship Studies of Strigolactone-Related Molecules for Branching Inhibition in Garden Pea: Molecule Design for Shoot Branching. Plant Physiol. 2012; 159:1524–1544. [PubMed: 22723084]
22. Waters MT, et al. A *Selaginella moellendorffii* Ortholog of KARRIKIN INSENSITIVE2 Functions in Arabidopsis Development but Cannot Mediate Responses to Karrikins or Strigolactones. Plant Cell. 2015; 27:1925–1944. [PubMed: 26175507]
23. Yang Y, et al. Inactive methyl indole-3-acetic acid ester can be hydrolyzed and activated by several esterases belonging to the AtMES esterase family of Arabidopsis. Plant Physiol. 2008; 147:1034–1045. [PubMed: 18467465]
24. Boyer F-D, et al. New Strigolactone Analogs as Plant Hormones with Low Activities in the Rhizosphere. Mol. Plant. 2014; 7:675–690. [PubMed: 24249726]
25. Shi W, Ma H. Spectroscopic probes with changeable pi-conjugated systems. Chem. Commun. 2012; 48:8732–8744.
26. Sun WC, Gee KR, Haugland RP. Synthesis of novel fluorinated coumarins: Excellent UV-light excitable fluorescent dyes. Bioorg. Med. Chem. Lett. 1998; 8:3107–3110. [PubMed: 9873685]
27. Dun EA, de Saint Germain A, Rameau C, Beveridge CA. Dynamics of Strigolactone Function and Shoot Branching Responses in Pisum sativum. Mol. Plant. 2013; 6:128–140. [PubMed: 23220942]
28. Fenaille F, Guy PA, Tabet J-C. Study of protein modification by 4-hydroxy-2-nonenal and other short chain aldehydes analyzed by electrospray ionization tandem mass spectrometry. J. Am. Soc. Mass Spectrom. 2003; 14:215–226. [PubMed: 12648928]
29. Chevalier F, et al. Strigolactone Promotes Degradation of DWARF14, an alpha/beta Hydrolase Essential for Strigolactone Signaling in Arabidopsis. Plant Cell. 2014; 26:1134–1150. [PubMed: 24610723]
30. Gutjahr C, et al. Rice perception of symbiotic arbuscular mycorrhizal fungi requires the karrikin receptor complex. Science. 2015; 350:1521–1524. [PubMed: 26680197]
31. Conn CE, et al. Convergent evolution of strigolactone perception enabled host detection in parasitic plants. Science. 2015; 349:540–543. [PubMed: 26228149]
32. Lopez-Obando M, et al. Structural modelling and transcriptional responses highlight a clade of PpKAI2-LIKE genes as candidate receptors for strigolactones in *Physcomitrella patens*. Planta. 2016

33. Toh S, et al. Structure-function analysis identifies highly sensitive strigolactone receptors in *Striga*. Science. 2015; 350:203–207. [PubMed: 26450211]
34. Arumingtyas EL, Floyd FS, Gregory MJ, Murfet IC. Branching in *Pisum*: inheritance and allelism tests with 17 *ramosus* mutants. Pisum Genet. 1992; 24:17–31.
35. Rameau C, et al. New *ramosus* mutants at loci *Rms1*, *Rms3* and *Rms4* resulting from the mutation breeding program at Versailles. Pisum Genet. 1997; 29:7–12.
36. Symons GM, Murfet IC. Inheritance and allelism tests on six further branching mutants in pea. Pisum Genet. 1997; 29:1–6.
37. Braun N, et al. The pea TCP transcription factor PsBRC1 acts downstream of Strigolactones to control shoot branching. Plant Physiol. 2012; 158:225–238. [PubMed: 22045922]
38. Sorefan K, et al. *MAX4* and *RMS1* are orthologous dioxygenase-like genes that regulate shoot branching in Arabidopsis and pea. Genes Dev. 2003; 17:1469–1474. [PubMed: 12815068]
39. Stirnberg P, van de Sande K, Leyser HMO. MAX1 and MAX2 control shoot lateral branching in Arabidopsis. Development. 2002; 129:1131–1141. [PubMed: 11874909]
40. Toh S, Holbrook-Smith D, Stokes ME, Tsuchiya Y, McCourt P. Detection of Parasitic Plant Suicide Germination Compounds Using a High-Throughput Arabidopsis HTL/KAI2 Strigolactone Perception System. Chem. Biol. 2014; 21:988–998. [PubMed: 25126711]
41. Karimi M, Bleys A, Vanderhaeghen R, Hilson P. Building blocks for plant gene assembly. Plant Physiol. 2007; 145:1183–1191. [PubMed: 17965171]
42. Clough SJ, Bent AF. Floral dip: a simplified method for Agrobacterium-mediated transformation of *Arabidopsis thaliana*. Plant J. 1998; 16:735–743. [PubMed: 10069079]
43. Laemmli UK. Cleavage of structural proteins during assembly of head of bacteriophage T-4. Nature. 1970; 227:680–685. [PubMed: 5432063]
44. Geoghegan KF, et al. Spontaneous alpha-N-6-phosphogluconoylation of a "His tag" in *Escherichia coli*: The cause of extra mass of 258 or 178 Da in fusion proteins. Anal. Biochem. 1999; 267:169–184. [PubMed: 9918669]
45. Sheldrick GM. A short history of SHELX. Acta Crystallogr., Sect. A. 2008; 64:112–122. [PubMed: 18156677]
46. Sheldrick GM. Crystal structure refinement with SHELXL. Acta Crystallogr., Sect. C. 2015; 71:3–8.
47. Drapeau GR, Boily Y, Houmard J. Purification and Properties of an Extracellular Protease of *Staphylococcus aureus*. J. Biol. Chem. 1972; 247:6720–6726. [PubMed: 4627743]
48. Kelley LA, Sternberg MJE. Protein structure prediction on the Web: a case study using the Phyre server. Nat. Protoc. 2009; 4:363–371. [PubMed: 19247286]
49. McNicholas S, Potterton E, Wilson KS, Noble MEM. Presenting your structures: the CCP4mg molecular-graphics software. Acta Crystallogr., Sect. D. 2011; 67:386–394. [PubMed: 21460457]
50. Worth CL, Preissner R, Blundell TL. SDM-a server for predicting effects of mutations on protein stability and malfunction. Nucleic Acids Res. 2011; 39:W215–W222. [PubMed: 21593128]
51. Tamura K, et al. MEGA5: Molecular Evolutionary Genetics Analysis Using Maximum Likelihood, Evolutionary Distance, and Maximum Parsimony Methods. Mol. Biol. Evol. 2011; 28:2731–2739. [PubMed: 21546353]
52. Schwarz, M.; Dayhoff, M. Dayhoff, M., editor. National Biomedical Research Foundation; Washington, DC: 1979. p. 353-358.
53. Fox J. The R commander: A basic-statistics graphical user interface to R. J. Stat. Softw. 2005; 14:1–42.

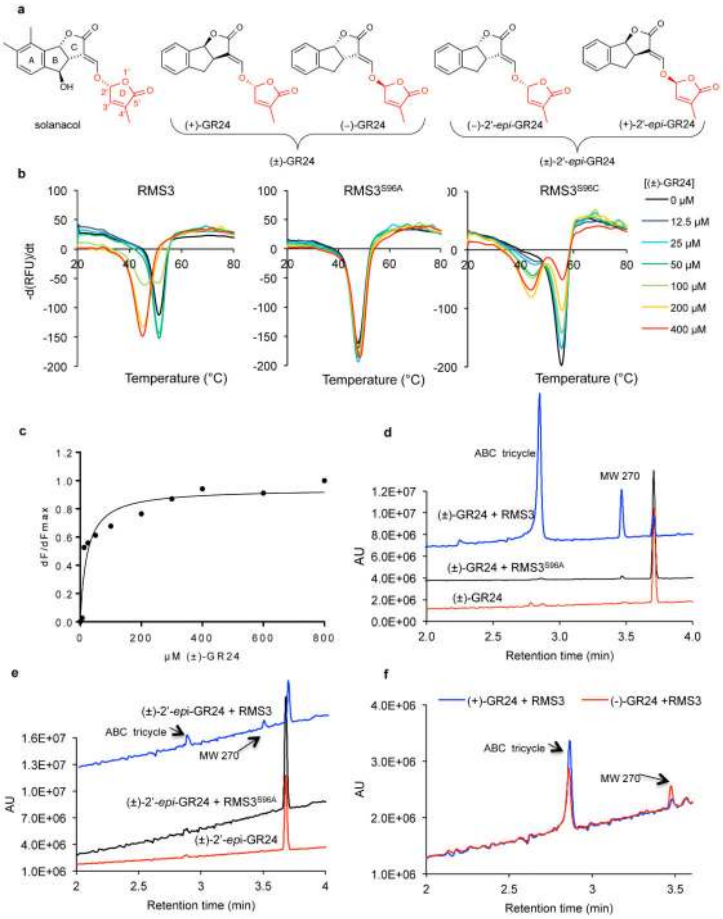

Figure 1. RMS3 can interact with and hydrolyze GR24 enantiomers and is stabilized by these compounds

(a) Chemical structures of one natural strigolactone, (±)-solanacol, and GR24 stereoisomers. (**b**) Melting temperature curves of RMS3 and mutant proteins in the presence of different concentrations of (±)-GR24, as assessed by differential scanning fluorimetry (DSF). Each line represents the average protein melt curve for three technical replicates and the experiment was carried out twice. (**c**) Titration of RMS3 interaction with (±)-GR24, monitored by intrinsic fluorescence at 340 nm. Changes in fluorescence were used to calculate the dissociation coefficient (K_d) of (±)-GR24 with RMS3. Each data point is the mean of two technical replicates. (**d-f**) Elution profile of the enzymatic assay with buffer, RMS3 or RMS3^{S96A} and GR24 analogs. UPLC-DAD (200–400 nm) analysis showing the formation of ABC and an unknown derivative (MW 270) (confirmed by mass spectrometry analyses) from (**d**) (±)-GR24, (**e**) (±)-2'-*epi*-GR24, and (**f**) (+)-GR24 and (−)-GR24. AU, absorbance unit. UPLC-DAD, ultra-performance liquid chromatography method with diode array detection. The chromatograms show representative results observed in two independent experiments with two technical replicates.

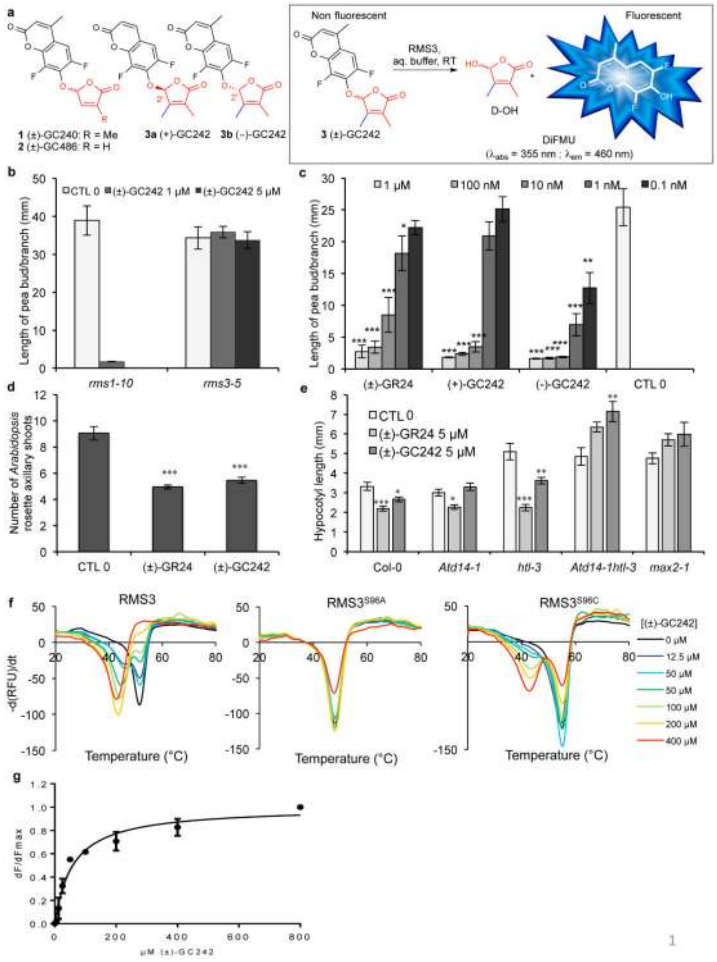

Figure 2. Characterization of the profluorescent probe (±)-GC242

(**a**) Chemical structures and principle of the profluorescent probe. (**b**) Length of the axillary bud for *rms1-10* and *rms3-5* pea plants, 8 days following direct application of (±)-GC242. Data are means ± SE (≥20 plants) (**c**) Axillary bud length for *rms1-10* pea plants, 8 days following direct application of (±)-GR24, (+)-GC242, (−)-GC242. Data are means ± SE (≥ 18 plants). Asterisks indicate significant differences from control values (***$p < 0.001$, ** $p < 0.01$, Kruskal-Wallis rank sum test). (**d**) Number of axillary shoots after hydroponic treatment of *max4-1 Arabidopsis* plants with (±)-GR24, (±)-GC242 (1 µM). Data are means ± SE (≥19 plants). (***$p < 0.001$, Kruskal-Wallis rank sum test). All experiments (**b**,**c**,**d**) were repeated twice. (**e**) *Arabidopsis* hypocotyl length in response to (±)-GR24 or (±)-GC242 of Col-0 (WT), *Atd14*-1, *htl-3*, *Atd14*-1 *htl-3*, and *max2-1 Arabidopsis* mutants. Data are means ± SE (≥10 plants). Asterisks indicate significant difference from corresponding acetone treatment (CTL) (***$p < 0.001$, ** $p < 0.01$, * $p < 0.05$, Student's t test). The experiments were repeated twice. (**f**) Melting temperature curves for RMS3 and mutant proteins at varying concentrations of (±)-GC242, as assessed by DSF. Each line represents the average protein melt curve for three replicate samples run in parallel. (**g**) Titration of RMS3 interaction with (±)-GC242 monitored by fluorescence. Each data point

is the mean ± SD of three technical replicates and three or four independent experiments, which gave similar results.

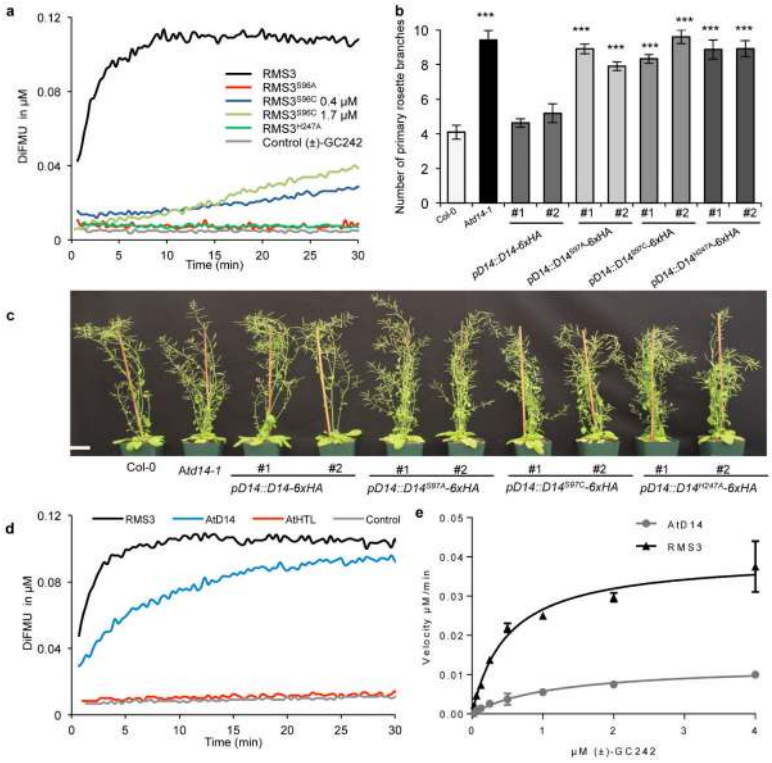

Figure 3. Enzymatic kinetics reveal that the serine and histidine of the catalytic triad are essential for RMS3 and AtD14 function

(**a,d-e**) Comparison of enzymatic kinetics when RMS3, AtD14, AtHTL, and different RMS3 mutant proteins were incubated with (±)-GC242. (**a**) Progress curves during (±)-GC242 hydrolysis. RMS3, RMS3^{S96A}, RMS3^{S96C} and RMS3^{H247A} catalyzed hydrolysis with 400 nM of protein (and 1700 nM for RMS3^{S96C}) and 500 nM of (±)-GC242. (**b-c**) Complementation of the *Atd14-1* mutant by different D14 mutant proteins. The *Atd14-1* mutant was transformed with a chimeric construct consisting of the native *D14* promoter fused to either the WT D14 coding sequence and a 6xHA tag (pD14::D14-6xHA), or an otherwise identical coding sequence in which Ser97 was mutated to Ala (pD14::D14^{S97A}-6xHA) or to Cys (pD14::D14^{S97C}-6xHA), and H247 was mutated to Ala (pD14::D14^{H247A}-6xHA). T2 segregating seeds were grown for 40 days. Data are means ± SE of at least 10 plants. Asterisks indicate significant difference from WT Col 0 (***$p <$ 0.001, Student's t test). Further methodological details are provided in Methods. Scale bar = 4 cm. The experiments were repeated twice. (**d**) Progress curves during (±)-GC242 hydrolysis. RMS3, AtD14, and AtHTL catalyzed hydrolysis with 400 nM of protein and 500 nM of (±)-GC242. (**e**) RMS3 and AtD14 pre-steady-state kinetics reaction velocity with (±)-GC242. (**a,d**) The progress curves show representative results observed in three independent experiments with three technical replicates. (**e**) Each data point is the mean ± SE of three technical replicates.

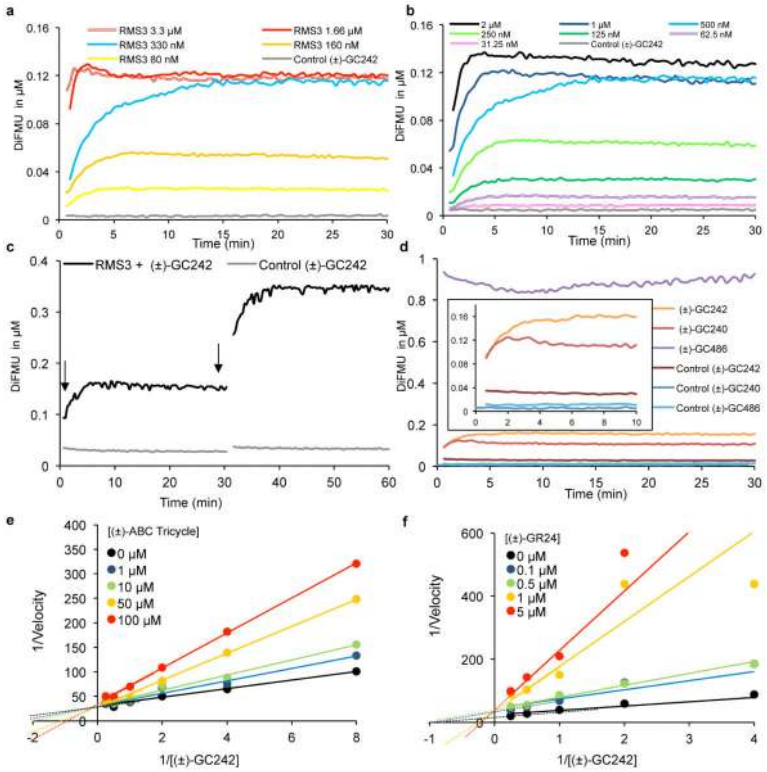

Figure 4. RMS3 acts as single turnover enzyme

(**a-d**) DiFMU concentration progress curves during (±)-GC242 hydrolysis. The release of DiFMU was monitored (λ_{em} 460 nm) at 25 °C. The progress curves show representative results observed in two independent experiments with two technical replicates. (**a**) RMS3-catalyzed hydrolysis of (±)-GC242 with different substrate concentrations in the presence of 400 nM protein. (**b**) RMS3-catalyzed hydrolysis with different protein concentrations and (±)-GC242 (500 nM). (**c**) (±)-GC242 (500 nM) hydrolysis with 2 successive additions of RMS3 protein (400 nM). Black arrows indicate protein additions. (**d**) (±)-GC486 (1 µM) hydrolysis with RMS3 protein (330 nM) versus (±)-GC242 and (±)-GC240 (1 µM) hydrolysis with RMS3 protein. **(e**) Effect of (±)-ABC tricycle on the enzyme kinetics of RMS3 shown as a Lineweaver–Burk plot. **(f**) Effect of (±)-GR24 on the enzyme kinetics of RMS3 shown as a Lineweaver–Burk plot. These plots were used to determine the K_i value. **(e-f**) Each data point is the mean ± SE of three technical replicates.

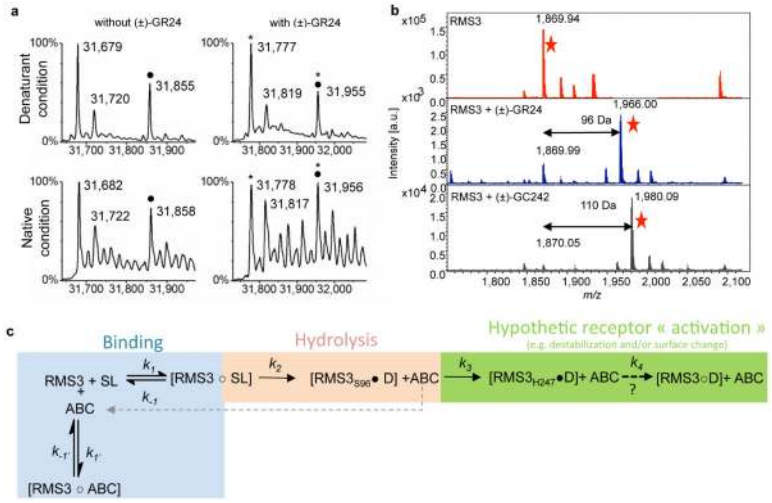

Figure 5. Formation of a stable RMS3-D-ring complex

(**a**) Mass spectra of RMS3 and RMS3-D-ring complex. Deconvoluted electrospray mass spectra of RMS3 before and after addition of (±)-GR24 (500 μM final concentration) in denaturant and native conditions. Peaks with an asterisk correspond to RMS3 covalently bound to D-ring (RMS3-D). The mass increment of 98 ± 2 Da in denaturant condition and 96 ± 2 Da in native condition measured for RMS3-GR24. Bold circle indicates RMS3 modified with a-N-Gluconoylation. Different unannotated peaks correspond to Na^+ adducts. (**b**) Mass spectra of the peptides (GHLPHLSAPSYLAHQLE (266-281) (246-262 in RMS3)) obtained after digestion of RMS3-HIS, RMS3-HIS + (±)-GR24, RMS3-HIS + (±)-GC242 by endoproteinase gluC. [a.u.], arbitrary unit. (**c**) Proposed kinetic mechanism for SL perception. [ ] = complex, black dot (?) symbolizes a covalent interaction and white dot (○) a non–covalent interaction. For $RMS3_x$, subscript indicates the amino acid involved in the covalent interaction, k_y = association constant and k_{-y} = dissociation constant. Double arrows indicate equilibrium and single arrows an irreversible reaction. Dotted arrows indicate hypothetical step. The grey arrow indicates the hypothetical product inhibition. The release of the ABC tricycle has been arbitrarily indicated during the first step of the hydrolysis.

Table 1

Thermodynamic and kinetic constants of ligands and probes toward RMS3

Protein	**RMS3**							
Ligand	**(±)-GR24**	**(±)-2'-*epi*-GR24**	**(+)-GR24**	**(−)-GR24**	**(±)-solanacol**	**(±)-3'-Me-GR24**	**(±)-4'-desmethyl-2'-*epi*-GR24**	**(±)-ABC**
K_d (μM)	22.0 ± 4.8	71.0 ± 15.2	15.7 ± 3.7	35.9 ± 3.6	137.1 ± 33.2	30.9 ± 5.2	295.7 ± 27.9	271.2 ± 29.8
K_i(μM)	0.10 ± 0.07	0.23 ± 0.03	0.07 ± 0.01	5.17 ± 1.01	21.5 ± 2.6	n.d.	n.d.	28.8 ± 17.6
Protein	**RMS3**						**AtD14**	
Probe	**(±)-GC242**	**(−)-GC242**	**(+)-GC242**	**(±)-GC240**	**(±)-GC486**	**DiFMU**	**(±)-GC242**	
K_d (μM)	58.9 ± 9.6	82.6 ± 7.6	581.1 ± 194.3	74.1 ± 5.9	21.0 ± 1.4	19.9 ± 1.1	n.d.	
$K_{1/2}$ (μM)	0.49 ± 0.05	1.56 ± 0.32	17.42 ± 4.17	3.83 ± 1.80	n.d.	n.d.	1.19 ± 0.21	
k_{cat} (min^{-1})	0,012 ± 0.005	0.184 ± 0.017	0.136 ± 0.027	0.054 ± 0.015	n.d.	n.d.	0.030 ± 0.002	
$k_{cat}/K_{1/2}$ ($\mu M^{-1}.min^{-1}$)	0.024	0.118	0.007	0.014	n.d.	n.d.	0.025	

Binding properties of RMS3 protein in the presence of different SL analogues were estimated by the apparent dissociation coefficients (K_d) derived from intrinsic fluorescence measurements. *Ki* values were determined using a competition test with (±)-GC242. $K_{1/2}$ and k_{cat} are pre-steady-state kinetic constants for RMS3 and AtD14 with different profluorescent probes. n.d.: not determined. K_d values represent the mean (±SE) of two replicates and $K_{1/2}$, k_{cat} and *Ki* values represent the mean (±SE) of three replicates.